Aqueous humour dynamics in anterior chamber under influence of cornea indentation

Aqueous humour dynamics in anterior chamber under influence of cornea indentation

I Zuhaila[1], L Y Jiann[1], S Sharidan[1] and A Fitt[2]

[1] Department of Mathematical Sciences, Faculty of Science, Universiti Teknologi Malaysia, 81310 UTM Johor Bahru, Johor, Malaysia.
[2] Faculty of Technology, Design and Environment, Oxford Brookes University, Headington Campus, Gipsy Lane, Oxford, OX3 OBP, United Kingdom.

E-mail: zuhaila@utm.my

Abstract. The existing temperature different between the cornea and the pupil induces the aqueous humour (AH) to circulate in the anterior chamber (AC). The buoyancy forces produced by the temperature gradient has driven the AH to flow. Previous studies have shown that cornea indentation changes the structure of the AC. This imply that the cornea indentation may change the fluid flow behaviour in the AC. A mathematical model of AH flow has been developed in order to analyse the fluid mechanics concerning the indentation of the cornea. Naiver-Stokes equations is used to describe the flow of AH in the AC. The governing equations have been solved numerically using finite element method. The results show that the cornea indentation has slow down the circulation the AH in the AC.

1. Introduction

Buoyancy force due to temperature differences, secretory flow from the ciliary body through the pupil aperture and ultimately to the trabecular meshwork, and movement of the eye itself are the suggested mechanisms that drive the AH to flow in the AC [1]. A simple fluid dynamical models was used by the authors to study each of the mechanisms and the solutions was obtained by the aiding of asymptotic analysis methods. The authors concluded that the buoyancy induced by temperature gradient in the eye is the main mechanism for causing AC flow. Besides, [2] applied a simple standard fluid dynamical model to examine the flow in the AC which is driven by thermal processes. The formation of a hyphema or a Krukenberg spindle were predicted by them with the aiding of the model. They had justified that the buoyancy driven flows in the AC play a significant role and indicates that only very small temperature gradient are required to drive such flows. Further, a Boussinesq model of natural convection in the AC was developed by [3] in order to predict the magnitude of the natural convection flow of the AH. The model also used to estimate the movement of pigment particles in the AC. The lubrication theory was used by [2] in order to determine the analytical solutions of the governing equations, was not applied by [3]. However, [3] solved the model numerically with the help of FIDP computer package. The governing equations were formulated using the finite element method and the domain was divided into 27-node brick elements. The authors found a same results as shown in [2] that was the temperature gradients within the AC of the human eye are sufficient to create significant natural convection currents of AH. [4] used a commercial CFD package FLUENT to study the fluid dynamics of the AH in the AC of eye. In addition, the drainage mechanisms through the Trabecular Meshwork (TM) was also considered. The authors concluded that the buoyancy force is the dominant source to drive the AH flow.

[5], developed a 3D model of the human eye which include the TM, Schlemm's canal and collecting channels structures. The AH flow characteristics under physiological and pathological conditions such as primary open-angle glaucoma was simulated by ANSYS CFX (ANSYS Inc., Canonsburg, PA, USA). Recently, [6] developed a fluid mechanical model of buoyancy driven AH flow in the AC around Descemet Membrane Detachment (DMD) to investigate the spontaneous reattachment phenomena of the DMD. They concluded that, the clinical outcomes for DMDs were depended on the temperature difference across the eye.

On the other hand, a research was conducted by [7] to investigate the alteration of the angle between the iris and cornea and the change of the iris contour during indentation of cornea or sclera. The indentation of the cornea or sclera consequently rotate the iris root. Moreover, [8-11] had shown that the AC angle can be wider by indent the cornea. [12] extended their research to investigate the fluid structure interaction between the iris and AH, driven by iris root rotation due to the indentation of cornea or sclera. These indicate that the structure of the AC is changed when the cornea is indented, then it may alter the behaviour of the AH flow in the AC. However, there is limit discussion on the effect of the cornea indentation to the circulation of the AH driven by the temperature gradient in the AC. Therefore, the objective of this paper is to study the influence of the cornea indentation to the AH flow in AC numerically by using finite element method (FEM). Matlab software is utilized to compute and visualize the numerical solutions.

2. Mathematical formulation

AC is an approximately ellipsoidal shape region that bounded by the cornea, iris and lens, which has depth in range 2.5 to 3 [mm] and diameter in the plane of the iris root is in range 9 to 12 [mm] ([2, 4, 6, 13]). Hence, the AC is modelled as a "half-moon" shape as illustrated in figure 1 in this study. Besides, the diameter of the AC is assumed to be 11 [mm] and the depth to be 2.75 [mm] as follow [2, 6]. The iris is assumed as a rigid surface at the bottom and the curvature of the iris surface is neglected and assumed it as a flat plane. It is justified by [1, 2, 4, 6] that those assumptions incorporate insignificant error in the results. The circulation of AH in the AC is assumed mainly driven by the buoyancy forces. The temperature gradient between the iris and the cornea has generated the buoyant force to drive the AH. The temperature drop between the cornea and the iris is taken to be 2-4 [^{0}C] for the open eye ([2, 4, 6]). 98 % of the AH is built up by water and the other 2 % is made up by protein, several of amino acids, oxygen, lactate and glucose ([13, 14]). Thus, the density and viscosity of the AH is similar to water ([15, 16]).

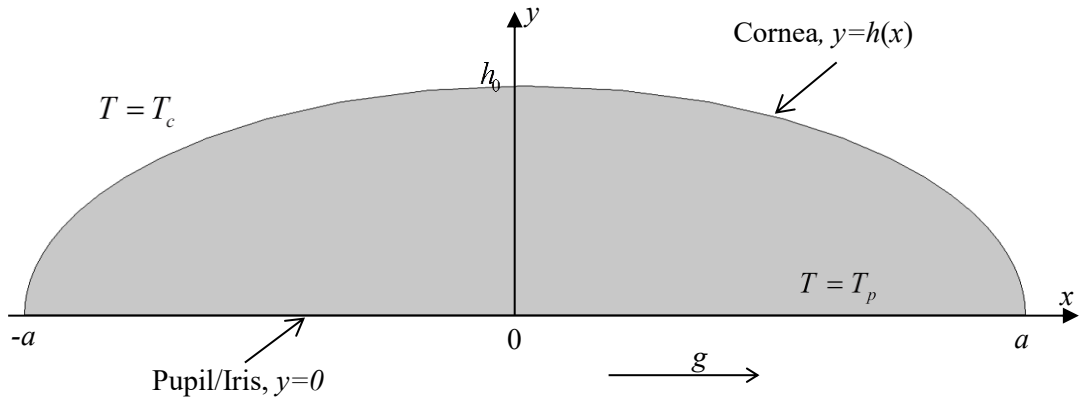

Figure 1. Schematic diagram of the AC.

In the plane $z = 0$, a two-dimensional AH flow driven by buoyancy effects in the AC has been considered, as shown in figure 1. The temperature at the back of the AC is assumed close to core body temperature (37 [^{0}C]). Due to the ambient temperature (say 25 [^{0}C]), the cornea is assumed to has

temperature 35 [^{0}C]. Therefore in Cartesian coordinate system (x, y), the AH is supposed flows between the plane formed by pupil aperture and the iris, $y = 0$ and the anterior surface of the cornea, $y = h(x)$. At the iris, the temperature is fixed at T_p which is close to the human body temperature, 37 [^{0}C], and the temperature at the cornea is assumed to be T_c, around 35 [^{0}C]. The gravity, g is acted along the positive x-axis as seen in figure 1. To be realistic, a set of typical values for human eye is used such as $h_0 = 2.75$ [mm], $a = 5.5$ [mm], gravity $g = 9.8$ [ms^{-2}] and the AH has a typical velocity of $U = 10^{-4}$[ms^{-1}], density $\rho = 1000$ [kgm^{-3}], viscosity $\mu = 0.9\times10^{-3}$ [kgm^{-1}s^{-1}], specific heat $c_P = 4200$ [Jkg^{-1}K^{-1}], thermal conductivity $k = 0.57$ [Wm^{-1}K^{-1}] and coefficient of thermal expansion $\beta = 3\times10^{-4}$ [K-1]. The AH is assumed to be Newtonian, viscous and incompressible. The governing equations are

$$\begin{aligned}
\frac{\partial u}{\partial x}+\frac{\partial v}{\partial y}&=0,\\
\rho\left(u\frac{\partial u}{\partial x}+v\frac{\partial u}{\partial y}\right)+\frac{\partial P}{\partial x}-\mu\left(\frac{\partial^2 u}{\partial x^2}+\frac{\partial^2 u}{\partial y^2}\right)+g\rho\beta\left(T-T_\infty\right)&=0,\\
\rho\left(u\frac{\partial v}{\partial x}+v\frac{\partial v}{\partial y}\right)+\frac{\partial P}{\partial y}-\mu\left(\frac{\partial^2 v}{\partial x^2}+\frac{\partial^2 v}{\partial y^2}\right)&=0,\\
c_P\rho\left(u\frac{\partial T}{\partial x}+v\frac{\partial T}{\partial y}\right)-k\left(\frac{\partial^2 T}{\partial x^2}+\frac{\partial^2 T}{\partial y^2}\right)&=0.
\end{aligned} \tag{1}$$

Following [2], the boundary conditions are

$$\begin{aligned}
u(x,0)=v(x,0)&=0,\\
u\left(x,h(x)\right)=v\left(x,h(x)\right)&=0,\\
T(x,0)=T_p,\ T\left(x,h(x)\right)&=T_c,\\
P(a,0)&=P_a,
\end{aligned} \tag{2}$$

where P_a is the normal atmospheric pressure and equal to 101325 [Pa]. FEM is applied to solve equation (1) with subjected to the boundary conditions (2). To the best of authors' knowledge, the application of the finite element analysis to solve this problem is not yet adequately provided. Initially, the domain is discretized into nonuniform and unstructured triangular Taylor-Hood elements ([17-19]) and in each finite element e_i, $i = 1,2,\ldots n,$ the variables u^{e_i}, v^{e_i}, T^{e_i} and P^{e_i} are approximated as

$$\begin{aligned}
u=u^{e_i}&=\phi_j^{e_i}(x,y)\,u_j^{e_i},\ j=1,2,\ldots,6.\\
v=v^{e_i}&=\phi_j^{e_i}(x,y)\,v_j^{e_i},\ j=1,2,\ldots,6.\\
P=P^{e_i}&=\psi_k^{e_i}(x,y)\,P_k^{e_i},\ k=1,2,3.\\
T=T^{e_i}&=\phi_j^{e_i}(x,y)\,v_j^{e_i},\ j=1,2,\ldots,6.
\end{aligned} \tag{3}$$

where, $\phi_j^{e_i}$ and $\psi_k^{e_i}$ are the shape functions for the dependent variables velocity, temperature and the pressure respectively. Galerkin finite element methods is practiced in this study. After discretises the equations (1) by the method, the equations (1) can be represented in a matrix form as

$$\begin{bmatrix} S_{11} & S_{12} & S_{13} & S_{14} \\ S_{21} & S_{22} & S_{23} & S_{24} \\ S_{31} & S_{32} & S_{33} & S_{34} \\ S_{41} & S_{42} & S_{43} & S_{44} \end{bmatrix} \begin{Bmatrix} \{u_j^{e_i}\}^T \\ \{v_j^{e_i}\}^T \\ \{P_k^{e_i}\}^T \\ \{T_j^{e_i}\}^T \end{Bmatrix} = \begin{bmatrix} r_1 \\ r_2 \\ r_3 \\ r_4 \end{bmatrix}, \tag{4}$$

where

$$S_{11} = \left[\int_{A_{e_i}} \begin{matrix} \{\phi_l^{e_i}\} \rho \left(u^{e_i} \dfrac{\partial \{\phi_j^{e_i}\}}{\partial x} + v^{e_i} \dfrac{\partial \{\phi_j^{e_i}\}}{\partial y} \right) \\ + \mu \left(\dfrac{\partial \{\phi_l^{e_i}\}}{\partial x} \dfrac{\partial \{\phi_j^{e_i}\}}{\partial x} + \dfrac{\partial \{\phi_l^{e_i}\}}{\partial y} \dfrac{\partial \{\phi_j^{e_i}\}}{\partial y} \right) \end{matrix} dA_{e_i} \right]$$

$$S_{12} = S_{21} = S_{24} = S_{41} = S_{42} = [0]_{6\times 6},\ S_{13} = \left[\int_{A_{e_i}} \{\phi_l^{e_i}\} \frac{\partial \{\psi_k^{e_i}\}}{\partial x} dA_{e_i} \right],$$

$$S_{14} = \int_{A_{e_i}} \{\phi_l^{e_i}\} g \rho \beta \{\phi_j^{e_i}\} dA_{e_i},\ S_{22} = S_{11},$$

$$S_{23} = \left[\int_{A_{e_i}} \{\phi_l^{e_i}\} \frac{\partial \{\psi_k^{e_i}\}}{\partial y} dA_{e_i} \right],\ S_{31} = \left[\int_{A_{e_i}} \{\psi_m^{e_i}\} \frac{\partial \{\phi_j^{e_i}\}}{\partial x} dA_{e_i} \right],$$

$$S_{32} = \left[\int_{A_{e_i}} \{\psi_m^{e_i}\} \frac{\partial \{\phi_j^{e_i}\}}{\partial y} dA_{e_i} \right],\ S_{33} = [0]_{3\times 3}, S_{34} = [0]_{3\times 6},\ S_{43} = [0]_{6\times 3}$$

$$S_{44} = \left[\int_{A_{e_i}} \begin{matrix} \{\phi_l^{e_i}\} c_P \rho \left(u^{e_i} \dfrac{\partial \{\phi_j^{e_i}\}}{\partial x} + v^{e_i} \dfrac{\partial \{\phi_j^{e_i}\}}{\partial y} \right) \\ + k \left(\dfrac{\partial \{\phi_l^{e_i}\}}{\partial x} \dfrac{\partial \{\phi_j^{e_i}\}}{\partial x} + \dfrac{\partial \{\phi_l^{e_i}\}}{\partial y} \dfrac{\partial \{\phi_j^{e_i}\}}{\partial y} \right) \end{matrix} dA_{e_i} \right]$$

$$r_1 = \oint_{\Gamma_{e_i}} \mu \left(\{\phi_l^{e_i}\} \frac{\partial \phi_j^{e_i} u_j^{e_i}}{\partial x} n_x + \{\phi_l^{e_i}\} \frac{\partial \phi_j^{e_i} u_j^{e_i}}{\partial y} n_y \right) d\Gamma_{e_i} + \int_{A_{e_i}} \phi_l^{e_i} g \rho \beta T_\infty dA_{e_i},$$

$$r_2 = \oint_{\Gamma_{e_i}} \mu \left(\{\phi_l^{e_i}\} \frac{\partial \phi_j^{e_i} v_j^{e_i}}{\partial x} n_x + \{\phi_l^{e_i}\} \frac{\partial \phi_j^{e_i} v_j^{e_i}}{\partial y} n_y \right) d\Gamma_{e_i},\ r_3 = [0]_{3\times 1},$$

$$r_4 = \oint_{\Gamma_{e_i}} k \left(\{\phi_l^{e_i}\} \frac{\partial \phi_j^{e_i} T_j^{e_i}}{\partial x} n_x + \{\phi_l^{e_i}\} \frac{\partial \phi_j^{e_i} T_j^{e_i}}{\partial y} n_y \right) d\Gamma_{e_i},$$

and

$$\left\{\phi_j^{e_i}\right\}=\left\{\phi_1^{e_i} \quad \phi_2^{e_i} \quad \phi_3^{e_i} \quad \phi_4^{e_i} \quad \phi_5^{e_i} \quad \phi_6^{e_i}\right\},$$
$$\left\{\psi_k^{e_i}\right\}=\left\{\psi_1^{e_i} \quad \psi_2^{e_i} \quad \psi_3^{e_i}\right\},$$
$$\left\{u_j^{e_i}\right\}^T=\left\{u_1^{e_i} \quad u_2^{e_i} \quad u_3^{e_i} \quad u_4^{e_i} \quad u_5^{e_i} \quad u_6^{e_i}\right\}^T,$$
$$\left\{v_j^{e_i}\right\}^T=\left\{v_1^{e_i} \quad v_2^{e_i} \quad v_3^{e_i} \quad v_4^{e_i} \quad v_5^{e_i} \quad v_6^{e_i}\right\}^T,$$
$$\left\{T_j^{e_i}\right\}^T=\left\{T_1^{e_i} \quad T_2^{e_i} \quad T_3^{e_i} \quad T_4^{e_i} \quad T_5^{e_i} \quad T_6^{e_i}\right\}^T,$$
$$\left\{P_j^{e_i}\right\}=\left\{P_1^{e_i} \quad P_2^{e_i} \quad P_3^{e_i}\right\}^T,$$
$$\left\{\phi_l^{e_i}\right\}=\left\{\phi_j^{e_i}\right\}^T,\ \left\{\psi_m^{e_i}\right\}=\left\{\psi_k^{e_i}\right\}^T.$$

Assembly the element matrix (4) for each finite element into a global matrix and then determine the solutions by solving the global matrix with subjecting to the boundary conditions (2). Nevertheless, the global matrix is a nonlinear system since equation (4) is nonlinear, thus it is needed to solve the system in an iteration manner. Newton-Raphson methods is applied to solve the global nonlinear system.

On the others hand, in [7] four kind of cornea indentation had considered. As an early stage of the study, only one of the instance is proposed in this paper which is the manual indentation of the central cornea. In addition, this nature of indentation obey the assumption of the iris surface as a flat plane. Generally, squint hook, cotton bud, glass rod, and gonioprism are the instruments used by the ophthalmologist to indent the central or peripheral surface of the cornea. However in this paper, a glass rod, which has 7 [mm] diameter is used to indent the central of cornea as shown in figure 2(a). This specific diameter is used so that the indentation formed with depth *d*, in range 0 to 0.5 [mm] always produces a flat indention on the surface of the cornea (see figure 2(b)). The consequence of the indentation to the fluid flow of the AH in the AC is investigated.

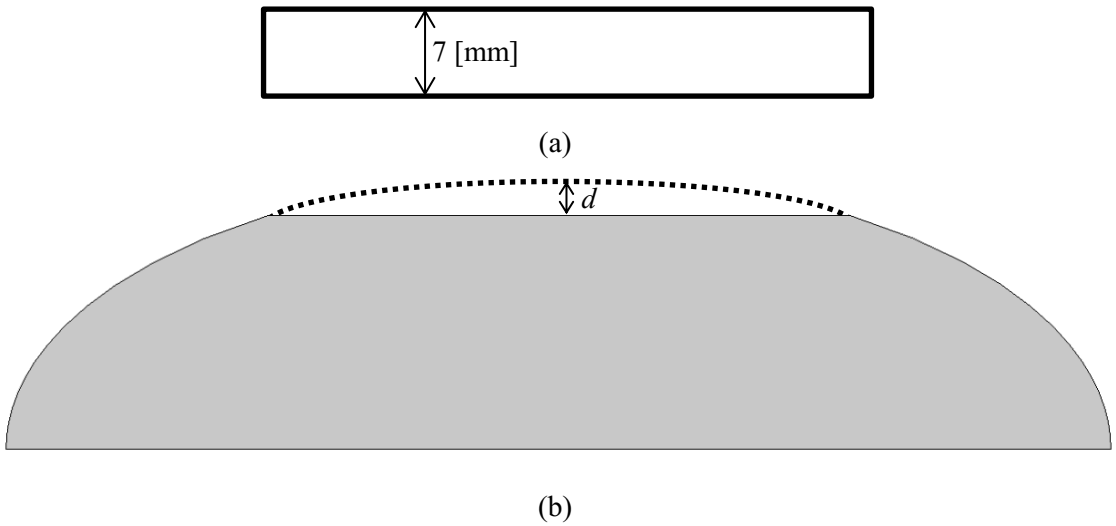

Figure 2. (a) A glass rod and (b) the indentation of the central cornea by the rod.

3. Results and discussion

A Matlab coding was developed to compute the numerical results and a personal computer with a processor speed of 2.30 GHz and a RAM of 8GB was used to run all the computation in the study. A mesh test was conducted first in order to show that the results is independent from the total number of elements used to mesh the domain. Figure 3 shows the *u*-velocity profiles along a vertical line passing

through the geometric center of the cornea with total number of elements 6413, 7374, 8546, 9266 and 10224 respectively. The figure illustrates that the results are excellent match. Therefore, we have shown that the results do not depend on the number of elements used. For the following study, the domain is meshed with 8000-10000 elements, 19000-20000 nodes and contained 60000-70000 degreed of freedoms. In other word, the global stiffness matrix that produced by the sources code are in size between 60000×60000 - 70000×70000.

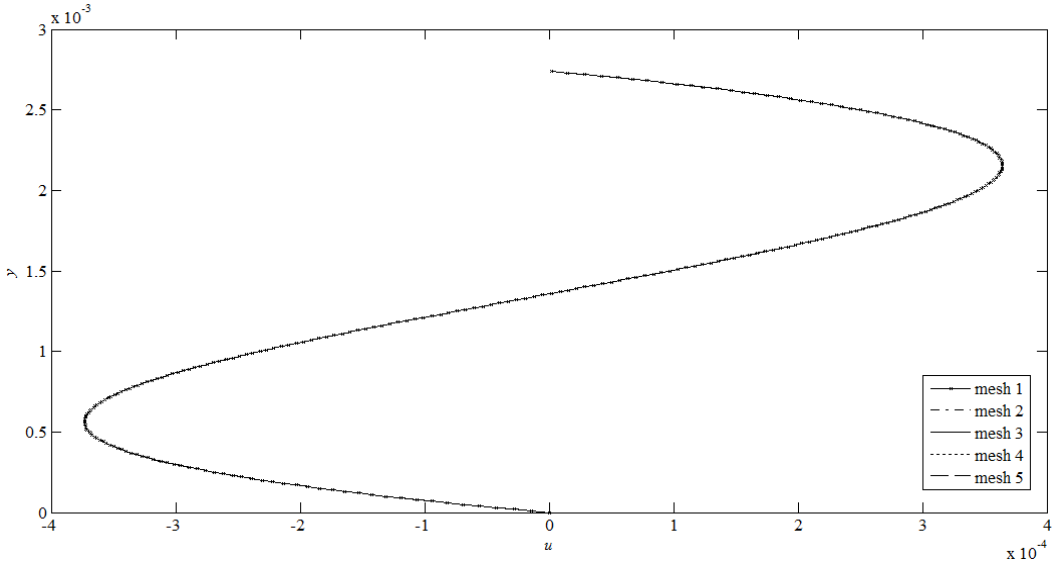

Figure 3. The *u*-velocity profiles along a vertical line passing through the geometric centre of the cornea with mesh 1 = 6413 elements, mesh 2 = 7374 elements, mesh 3 = 8546 elements, mesh 4 = 9266 elements and mesh 5 = 10224 elements.

Table 1 has shown the result of maximum *u*-velocity and the locations in the AC with the given results in [2, 6]. A slightly different between the results is illustrated in the table but it is in an acceptable range and may say it is in a great agreement. The quantitative agreement is very encouraging and has enhanced the confidence to the correctness of the obtained solutions. Besides that, Comsol Multiphysics, which is a commercial software applying FEM, was also used to simulate the fluid flow. 8848 elements were generated to mesh the domain and the solutions are in a great agreement with the present result as seen in table 1. Moreover, Comsol Multiphysics was also used to plot the velocity contour for the fluid flow in AC. The results generated by the present computer code (see figure 4(a)) are concurrent to the results determined by the commercial software (see figure 4(b).

Table 1. Comparisons of the maximum *u*-velocity and its location in the AC for the present results with the previous obtained results in the literature.

	Location	maximum *u*-velocity
|Present| $\left(\times \mathbf{10^{-4}}\right)$	(0, 0.0005600)	3.71976
|[2]| $\left(\times \mathbf{10^{-4}}\right)$	(0, 0.0005775)	3.96000
|[6]| $\left(\times \mathbf{10^{-4}}\right)$	(0, 0.0005811)	3.96200
|Comsol| $\left(\times \mathbf{10^{-4}}\right)$	(0, 0.0005645)	3.80686

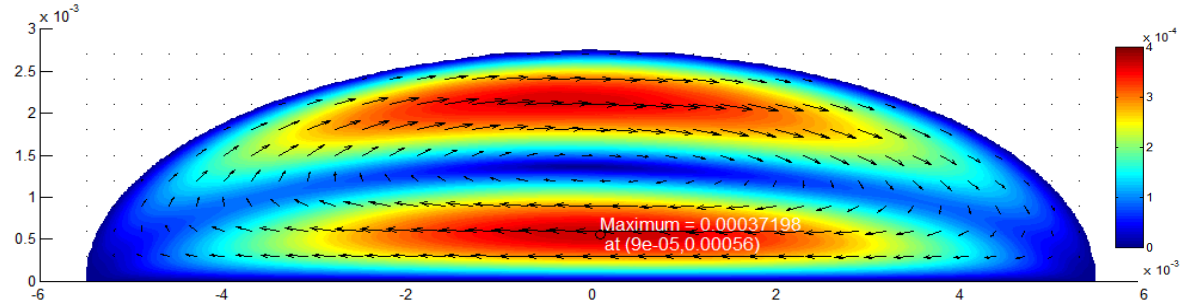

(a)

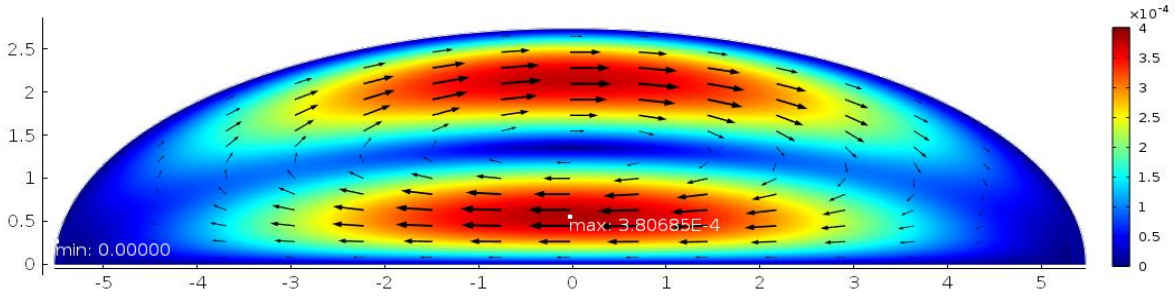

(b)

Figure 4. Velocity contour of the AH flow in the AC (a) Present (b) Comsol.

The effect of the cornea indentation to the behavior of the AH flow in AC are shown in figure 5. When comparing figure 5 with figure 4(a), the indentation decreases the maximum velocity magnitude in the AC. Moreover, the location of the maximum value exist also move upward near to the cornea as seen in Figure 5. Further, when *d* is increased from 0.3 [mm] to 0.5 [mm], the maximum velocity magnitude is slightly decreased. The location that the maximum velocity magnitude to be found is also changing and is moving further away to the left hand side of the *y*-axis. The results show that the scale effects which arises from difference in depth of the indentation, do effect the fluid behaviour in the human eye. [6] had stated that the position of the DMD and the fluid flow in AC do induce the spontaneous reattachment of the detached Descemet membrane. They concluded that the upper DMD, which the Descemet membrane is attached to the cornea above the centre of the cornea, are likely to naturally resolve themselves than lower DMD (the Descemet membrane is attached to the cornea below the centre of the cornea). As elaborated in [6], the normal pressure that act form the left hand side of the upper DMD is higher the other side, thus the detached Descemet membrane is pushing closer to the cornea. The indentation of the cornea has decrease the velocity of the AH flow in the AC, therefore, based on the Bernoulli principle the normal pressure the act on the left hand side of the upper DMD may increase. This possible increase the percentage of happening spontaneous attachment of the upper DMD. Further research is needed to fully understand the real mechanism of the AH flow with the DMD and then induce the attachment of the DMD. Besides, in this study only one type of indentation is considered and also the shape of the instrument used to indent the cornea may change the movement of the AH in the AC.

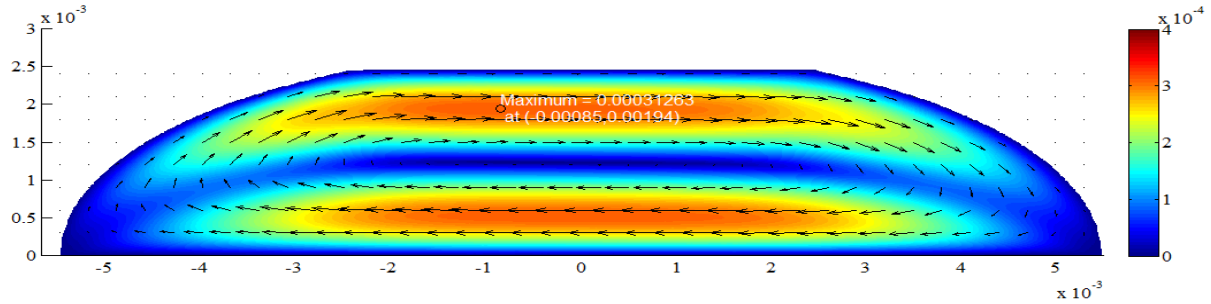

(a)

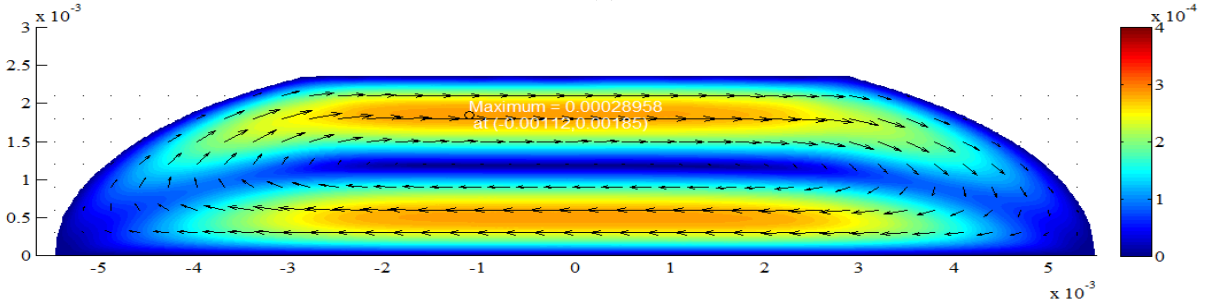

(b)

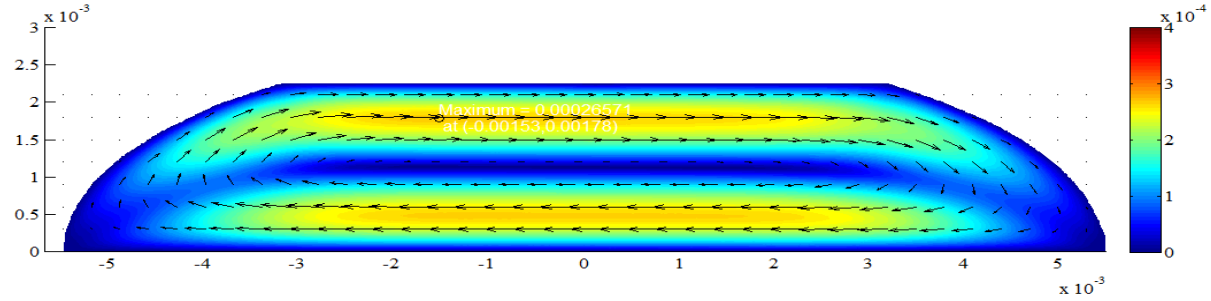

(c)

Figure 5. Velocity contour of the AH flow in the AC for the cornea indentation with depth *d*= (a) 0.3 [mm], (b) 0.4 [mm] and (c) 0.5 [mm].

4. Conclusions

The behaviour of the AH in the AC under the influence of the cornea indentation have been analyzed. Some figures are plotted to show the behaviour of the fluid under different depth of indentation. Some interesting finding of the study can be concluded as follows:

1. The velocity of the AH is effected by the depth of the indentation.
2. The computation model and the Matlab coding that developed in this study can be used to analyze the fluid flow in human eye with cornea indentation and also suggested to be applied to investigate a more advance research in the future.
3. The indentation of the cornea may increase the possibility of occurring the spontaneous reattachment of the DMD.

As suggestion, the fluid flow in the real shape of the AC and the effect of the shape of the indentation to the cornea should be considered in the future. Furthermore, the influence of the cornea indentation to the phenomena of the spontaneous attachment of DMD need further investigation.

Acknowledgments
The authors would like to acknowledge KPT (MyBrain), MoHE and Research Management Centre – UTM for the financial support through vote numbers 4F632, 4F713, 13H28, 13H74 and 03G53 for this research.

References
[1] Fitt A D and Gonzalez G 2006 *B. Math. Biol.* **68** 53-71
[2] Canning C R, Greaney M J, Dewynne J N and Fitt A D 2002 *IMA J. Math. Appl. Med.* **19** 31-60
[3] Heys J J and Barocas V H 2002 *Ann. Biomed. Eng.* **30** 392-401
[4] Kumar S, Acharya S, Beuerman R and Palkama A 2006 *Ann. Biomed. Eng.* **34** 530-44
[5] Villamarin A, Roy S, Hasballa R, Vardoulis O and Reymond P 2012 *Med. Eng. Phys.* **34** 1462-70
[6] Ismail Z, Fitt A D and Please C P 2013 *Math. Med. Biol.* **30** 1-17
[7] Amini R and Barocas V H 2009 *Invest. Ophth. Visual.* **50** 5288-94
[8] Forbes M 1966 *Arch Ophthalmol-Chic* **76** 488-92
[9] Anderson D R 1979 *Am. J. Ophthalmol.* **88** 1091-3
[10] Matsunaga K, Ito K, Esaki K, Sugimoto K, Sano T, Miura K, Sasoh M and Uji Y 2004 *Am. J. Ophthalmol.* **137** 552-4
[11] Masselos K, Bank A, Francis I C and Stapleton F 2009 *Ophthalmology* **116** 25-9
[12] Amini R and Barocas V 2010 *J. Biomed. Eng.* **132**
[13] Amini R 2010 *Iris Biomechanics in Health and Disease.* (The University Of Minnesota: Faculty of the Graduate School)
[14] Ethier C R, Johnson M and Ruberti J 2004 *Annu. Rev. Biomed. Eng.* **6** 249-73
[15] Scott J A 1988 *Phys. Med. Biol.* **33** 227-41
[16] Beswick J A and McCulloch C 1956 *Br. J. Ophthalmol.* **40** 545-8
[17] Reddy J N 2006 *An Introduction to the Finite Element Method* (Singapore: McGraw-Hill Education)
[18] Jichun L and Yi-Tung C 2008 *Computational Partial Differential Equations Using MATLAB* (Boca Raton: CRC Press)
[19] Zienkiewicz O C, Taylor R L and Zhu J Z 2005 *The Finite Element Method: Its Basis and Fundamentals: Its Basis and Fundamentals* (UK: Elsevier Science)